Crystal structure of $ZnWO_4$ scintillator material in the range of 3–1423 K

2009 J. Phys.: Condens. Matter 21 325402

(http://iopscience.iop.org/0953-8984/21/32/325402)

J. Phys.: Condens. Matter **21** (2009) 325402 (9pp) doi:10.1088/0953-8984/21/32/325402

Crystal structure of $ZnWO_4$ scintillator material in the range of 3–1423 K

D M Trots[1], A Senyshyn[2,3], L Vasylechko[3], R Niewa[4], T Vad[5], V B Mikhailik[6] and H Kraus[6]

[1] HASYLAB at DESY, Notkestrasse 85, D-22607 Hamburg, Germany
[2] Technische Universität Darmstadt, FB Material- und Geowissenschaften, Fachgebiet Strukturforschung, Petersenstrasse 23, D-64287 Darmstadt, Germany
[3] Lviv Polytechnic National University, Bandera Street 12, 79013 Lviv, Ukraine
[4] Department Chemie, Technische Universität München, Lichtenbergstrasse 4, 85747 Garching bei München, Germany
[5] Institut für Werkstoffwissenschaft, Technische Universität Dresden, Mommsenstrasse 13, 01062 Dresden, Germany
[6] Department of Physics, University of Oxford, Oxford OX1 3RH, UK

E-mail: d_trots@yahoo.com and Anatoliy.Senyshyn@frm2.tum.de

Received 4 February 2009, in final form 23 June 2009
Published 13 July 2009
Online at stacks.iop.org/JPhysCM/21/325402

Abstract

The behaviour of the crystal structure of $ZnWO_4$ was investigated by means of synchrotron and neutron powder diffraction in the range of 3–300 K. Thermal analysis showed the sample's melting around 1486 K upon heating and subsequent solidification at 1442 K upon cooling. Therefore, the structure was also investigated at 1423 K by means of neutron diffraction. It is found that the compound adopts the wolframite structure type over the whole temperature range investigated. The lattice parameters and volume of $ZnWO_4$ at low temperatures were parametrized on the basis of the first order Grüneisen approximation and a Debye model for an internal energy. The expansivities along the *a*- and *b*-axes adopt similar values and saturate close to 8×10^{-6} K^{-1}, whereas the expansion along the *c*-axis is much smaller and shows no saturation up to 300 K. The minimum expansivity corresponds to the direction close to the *c*-axis where edge-sharing linkages of octahedra occur.

1. Introduction

The continuous interest in zinc tungstate arises from its good scintillation properties which are the basis for the application of this material in industry and medicine as a detector of ionizing radiation. Recent interest in $ZnWO_4$ is motivated by its excellent prospect in experimental searches for rare events [1–3]. Therefore, zinc tungstate has become the subject of extensive research dedicated to detailed investigations of the optical properties of pure and doped $ZnWO_4$ and aiming to optimize its scintillation performance [4–8].

$ZnWO_4$, mineral name sanmartinite, belongs to a large group of monoclinic, divalent-transition-metal tungstates of the general formula AWO_4. The wolframite structure type, which can also be called $NiWO_4$-structure type, was assigned to $ZnWO_4$ first by Filipenko *et al* [9]. The structural model of zinc tungstate was improved in the work of Schofield *et al* [10], where Rietveld analysis was performed on neutron powder diffraction data obtained at ambient conditions. Several publications report effects of chemical doping on the structure of $ZnWO_4$-based solid solutions. In particular, high-temperature and composition dependence of the ferroelastic phase transition and room temperature structural distortion characteristics in $(Cu_xZn_{1-x})WO_4$ series were thoroughly investigated in [11–13]. Structural changes in the $Zn_{1-x}Cd_xWO_4$ system were determined in [14]: the deformation of the monoclinic wolframite structure towards the tetragonal scheelite (or $CaWO_4$-type) structure was found to be due to an increase in the deformation of the $(Zn, Cd)O_6$ and WO_6 octahedra with increasing Cd-content. Results on the effect of Ca doping on the structural and scintillation properties of $ZnWO_4$ are presented in [5]: due to a significant mismatch of the crystal structures of $CaWO_4$ and $ZnWO_4$ no mixing in the pseudo-binary $ZnWO_4$–$CaWO_4$ system was observed. Furthermore no structural phase transitions in $ZnWO_4$ were found down to 12 K and structure parameters at two selected temperatures (298 and 12 K) were reported [5].

Since a cryogenic detector has to be cooled down to very low temperatures, information about the thermal expansion

of $ZnWO_4$ is crucial with respect to the thermo-mechanical compatibility with other components of the detector. In order to characterize the structural behaviour of $ZnWO_4$ at low temperatures we investigated this material by synchrotron and neutron powder diffraction techniques over the temperature range 3–300 K. In addition, zinc tungstate was investigated at high temperatures by simultaneous thermal analysis and its structural parameters were refined at 1423 K using the neutron diffraction data.

2. Experimental details

The polycrystalline sample for the synchrotron diffraction experiments was synthesized via the solid state route. A sample of a $ZnWO_4$ scintillation crystal produced by Hilger Crystal (Margate, UK) was used for neutron diffraction experiments. The crystal structure of sample synthesized via the solid state route was the same as those of crystal commercially available. Further details regarding the samples and their characterization can be found elsewhere [4–6]. The simultaneous thermal analysis was performed on the commercial sample in air atmosphere using a NETZSCH STA 409 instrument. The sample was measured in the temperature range of 300–1573 K either in corundum or platinum crucibles at heating rates 10 or 5 K min^{-1}.

High resolution experiments were carried out at the synchrotron facility HASYLAB/DESY (Hamburg, Germany) at the powder diffraction beamline B2 [15]. The quartz capillary (0.3 mm in diameter and 35 mm in length) was completely filled with the powdered sample and sealed. The measurements were performed in Debye–Scherrer geometry using a closed-cycle helium cryostat [16] from Cryophysics, equipped with a capillary spinner. The wavelength of 0.499 60 Å was selected from the direct white synchrotron radiation beam using a Si(111) double flat-crystal monochromator. The wavelength was determined from eight reflection positions of LaB_6 reference material (NIST SRM 660a). Seventeen diffraction patterns were collected during continuous cooling down to 12 K using an on-site readable position-sensitive image-plate detector [17] in the 2θ range of 4.5°–40°.

Neutron powder diffraction data were collected at the structure powder diffractometer SPODI [18] installed at the research neutron reactor FRM-II (Garching near Munich, Germany). The powder sample was filled into a cylindrical can of 8 mm diameter, made from a thin (0.15 mm) vanadium foil and mounted into the closed-cycle cryostat. Thermal neutrons, after vertical focusing by a Ge(551) composite monochromator, were taken from the 155° take-off. The wavelength (1.5476 Å) was determined from the peak positions of Bragg reflections of silicon reference material (NIST SRM 640b). Seven full patterns were collected over a 2θ range of 10°–151° with a step size of 0.05° at temperatures of 3–300 K. High-temperature neutron diffraction was carried out using a high-temperature vacuum furnace equipped with a Nb heating element. The sample was contained in a cylindrical (8 mm in diameter) sample holder made of tantalum foil of 0.05 mm thickness. The temperature was measured simultaneously by two W/Re thermocouples and controlled with a EUROTHERM 2400™. The high-temperature setup was used to acquire data at 300 and 1423 K.

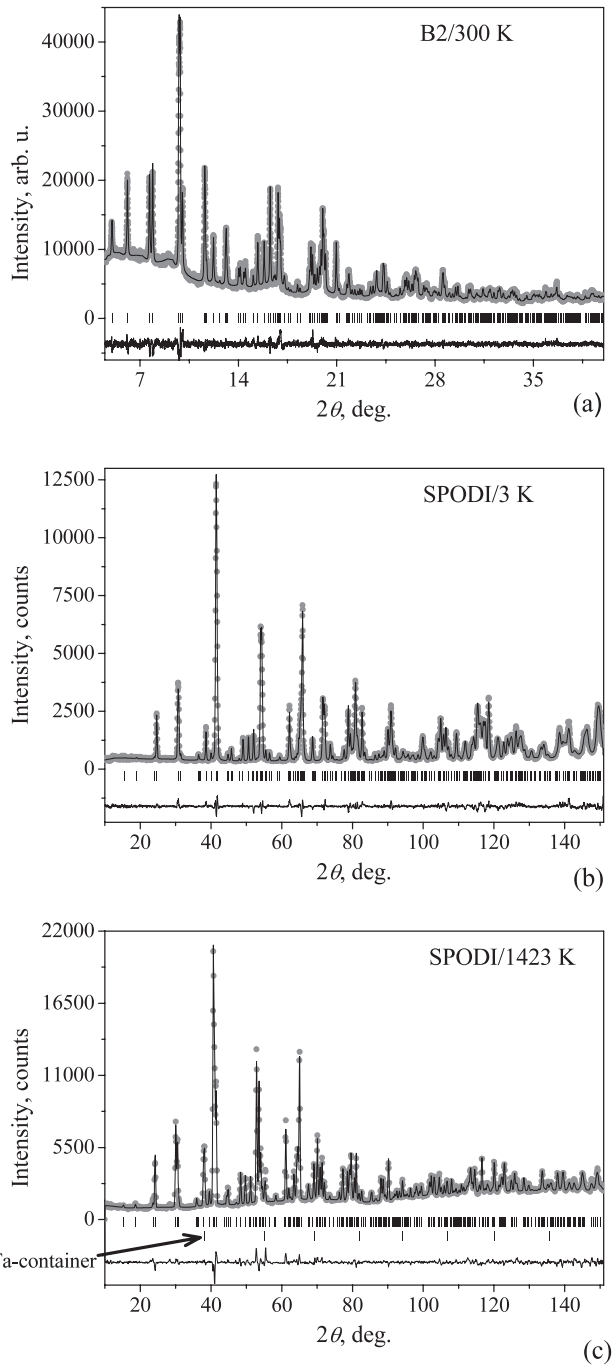

Figure 1. X-ray synchrotron at 300 K (a) and neutron at 3 K (b) and 1423 K (c) powder diffraction patterns of $ZnWO_4$, and model profiles from Rietveld refinements. Points are experimental data, the lines through the points represent calculated profiles and the curves at the bottom are differences between experimental and calculated profiles. The vertical ticks show the calculated positions of the Bragg peaks.

The data analysis was carried out using the FullProf suite of programs [19]. The peak profile shape was modelled by a pseudo-Voigt function. The background of the diffraction pattern was determined using a linear interpolation between selected data points in non-overlapping regions. The full-profile Rietveld method was applied for the analysis of the synchrotron and neutron data. The scale factor, lattice parameters, fractional coordinates of atomic sites

Table 1. Temperature evolution of the structure parameters of $ZnWO_4$ as obtained from the treatment of the neutron data by the Rietveld method. (Note: results of simultaneous treatment of neutron and synchrotron data at 300 K are presented in appendix.) The space group is $P2/c$ (No. 13), $Z = 2$. The structural data were modelled for the Zn cation occupying the 2f position with $x/a = 1/2$ and $z/c = 1/4$; W occupies the 2e position with $x/a = 0$ and $z/c = 1/4$.

T (K)		3	50	100	150	200	250	300	1423[a]
a (Å)		4.6829(1)	4.6830(1)	4.6839(1)	4.6853(1)	4.6872(1)	4.6888(1)	4.6902(1)	4.762 97(8)
b (Å)		5.7085(1)	5.7087(1)	5.7101(1)	5.7119(1)	5.7140(1)	5.7159(1)	5.7169(1)	5.7993(1)
c (Å)		4.9220(1)	4.9220(1)	4.9223(1)	4.9228(1)	4.9237(1)	4.9250(1)	4.9268(1)	4.974 38(8)
β (deg)		90.543(1)	90.546(1)	90.558(1)	90.574(1)	90.589(1)	90.606(1)	90.626(1)	91.175(1)
V (Å^3)		131.57(1)	131.58(1)	131.64(1)	131.74(1)	131.86(1)	131.99(1)	132.14(1)	137.37(1)
Zn, 2f	y/b	0.6827(3)	0.6822(3)	0.6828(3)	0.6828(3)	0.6835(3)	0.6833(3)	0.6838(4)	0.6911(8)
	B_{iso} (Å^2)	0.05(3)	0.07(3)	0.12(3)	0.23(3)	0.34(3)	0.42(3)	0.48(4)	3.8(2)
W, 2e	y/b	0.1815(4)	0.1810(4)	0.1810(4)	0.1809(4)	0.1811(4)	0.1815(4)	0.1820(4)	0.1849(7)
	B_{iso} (Å^2)	0.20(4)	0.22(4)	0.31(4)	0.33(4)	0.28(4)	0.31(4)	0.36(4)	1.9(2)
O1, 4g	x/a	0.2167(2)	0.2165(2)	0.2165(2)	0.2165(2)	0.2165(2)	0.2165(2)	0.2171(3)	0.2147(4)
	y/b	0.8947(2)	0.8952(2)	0.8954(2)	0.8950(2)	0.8952(2)	0.8952(2)	0.8953(2)	0.8973(5)
	z/c	0.4366(2)	0.4372(2)	0.4367(2)	0.4368(2)	0.4370(3)	0.4370(3)	0.4373(3)	0.4419(4)
	B_{iso} (Å^2)	0.19(2)	0.13(2)	0.19(2)	0.24(4)	0.30(2)	0.32(2)	0.42(2)	2.6(1)
O2, 4g	x/a	0.2565(2)	0.2565(2)	0.2564(2)	0.2566(2)	0.2560(3)	0.2561(3)	0.2557(3)	0.2523(5)
	y/b	0.3764(2)	0.3756(2)	0.3756(2)	0.3757(2)	0.3755(2)	0.3747(2)	0.3751(3)	0.3732(5)
	z/c	0.3995(2)	0.3999(3)	0.3997(3)	0.3999(3)	0.3995(3)	0.3996(3)	0.3999(3)	0.3982(4)
	B_{iso} (Å^2)	0.13(2)	0.18(2)	0.16(2)	0.24(2)	0.29(2)	0.33(2)	0.44(2)	2.9(1)
R_p (%)		4.74	4.81	4.81	4.82	4.78	4.72	4.74	3.68
R_{wp} (%)		5.81	5.89	5.86	5.87	5.86	5.74	5.82	4.76
χ^2		2.50	2.56	2.54	2.54	2.52	2.42	2.47	4.42

[a] Anisotropic ADP's in Å^2 at 1423 K: Zn— $B_{11} = 2.9(1)$, $B_{22} = 6.9(3)$, $B_{33} = 1.7(1)$, $B_{13} = 0.5(1)$; W— $B_{11} = 2.0(1)$, $B_{22} = 2.8(2)$, $B_{33} = 0.81(1)$, $B_{13} = 0.3(1)$; O1— $B_{11} = 2.0(1)$, $B_{22} = 4.7(1)$, $B_{33} = 1.1(1)$, $B_{12} = 0.2(1)$, $B_{13} = 0.8(1)$, $B_{23} = 0.5(1)$; O2— $B_{11} = 2.2(1)$, $B_{22} = 4.4(1)$, $B_{33} = 2.2(1)$, $B_{12} = -0.4(1)$, $B_{13} = -0.5(1)$, $B_{23} = -0.3(1)$.

and their isotropic atomic displacement parameters or ADP's (anisotropic only for the data collected at 1423 K), zero angular shift and profile shape parameters were varied during the fitting procedure. The standard absorption correction procedure for cylindrical samples, which is implemented in the 'FullProf' package, was applied.

3. Results and discussion

3.1. Low-temperature structural behaviour

The inspection of systematic absences of reflections in the powder diffraction patterns of $ZnWO_4$ collected at ambient conditions confirmed the monoclinic $P2/c$ symmetry, i.e., the wolframite structure type. Thus, the initial Rietveld refinements were based on the wolframite structure model. The graphical representation of the quality of the fits is shown in figure 1. The structural parameters of $ZnWO_4$, as obtained from neutron powder diffraction data, are summarized in table 1, while structural parameters obtained from synchrotron diffraction studies can be found elsewhere [5]. A detailed comparison of the $ZnWO_4$ cell dimensions at ambient conditions can be found in earlier publications [5, 10, 20], and is therefore not included in this work.

Despite the application of x-ray single crystal [14] and neutron [10, 13] powder diffraction techniques for the structural investigation of $ZnWO_4$, only isotropic ADP's were used by the authors for the refinement of the structure model. Therefore we performed structure refinements with anisotropic ADP's which resulted in a negative anisotropic temperature parameter B_{33} of the tungsten site. The negative B_{33} might indicate either a structural modulation or a slight difference from the $P2/c$ symmetry. However, since additional (modulated) reflections were observed neither in synchrotron nor in neutron diffraction patterns, we performed structure refinements using anisotropic ADP's and Pc, $P2$ and $P\bar{1}$ symmetries, which are maximal subgroups of $P2/c$. No convergence was achieved in case of the $P2$ symmetry, whereas the model based on $P\bar{1}$ quickly converged after some iterations giving similar goodness-of-fit values and also a negative B_{33} parameter of tungsten similar to that of the $P2/c$ symmetry. Despite the convergence of the model based on the Pc space group, anomalously short Zn–O and W–O distances were obtained. An attempt to apply anharmonic ADP's has been found to be equally unsuccessful. In addition, an attempt to model the W disorder residing at the 2e site (0, 0.1815(4), 1/4) by splitting this position to 4g crystallographic positions at (0.0083(14), 0.1832(4), 0.2127(7)) was undertaken which, however, resulted in a negative B_{33} of tungsten as well. Hence, only isotropic ADP's were used in our structural model. The reason for this unexpected behaviour of the anisotropic ADP's in $ZnWO_4$ remains unclear.

The $ZnWO_4$ structure is illustrated schematically in figure 2. It can be considered as a chain structure adopting zigzag chains formed of either edge-sharing ZnO_6 or edge-sharing WO_6 octahedra, which run parallel to the c-axis. Each WO_6 (or ZnO_6) octahedron shares two edges with two other neighbouring WO_6 (ZnO_6) octahedra in the chain. Each chain of ZnO_6 octahedra is corner-linked to four chains of WO_6 octahedra and vice versa. Moreover, open channels parallel to the c-axis are also present in the structure. Both ZnO_6 and WO_6 octahedra possess three pairs of equivalent Zn–O

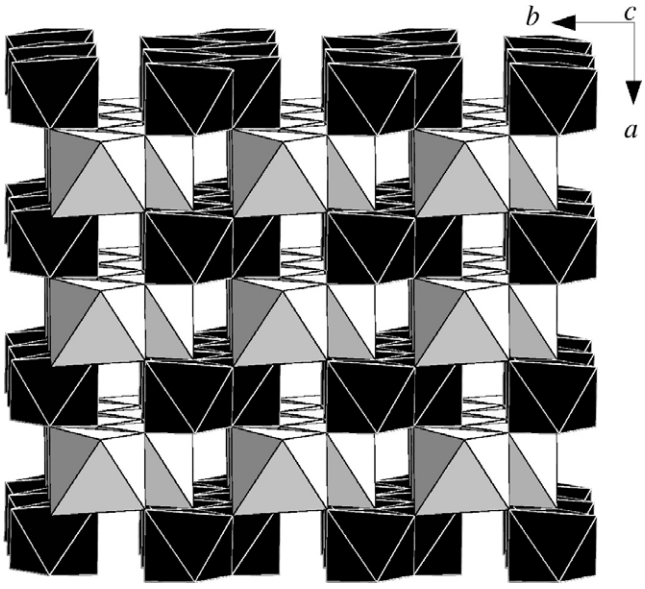

Figure 2. Crystal structure of $ZnWO_4$ viewed near the [001]-direction. Black and grey octahedra correspond to WO_6 and ZO_6, respectively.

Table 2. Pairs of Zn–O and W–O distances of octahedral ZnO_6 and WO_6 units resulting from the neutron diffraction experiments. All distances are given in Å.

T (K)	W–O1	W–O1	W–O2	Zn–O1	Zn–O2	Zn–O2
1423	1.920(2)	2.168(4)	1.773(4)	2.059(4)	2.123(2)	2.317(5)
300	1.908(1)	2.134(2)	1.784(2)	2.025(2)	2.088(1)	2.234(2)
250	1.906(1)	2.123(2)	1.785(2)	2.027(1)	2.087(1)	2.232(2)
200	1.904(1)	2.128(2)	1.788(2)	2.025(1)	2.088(1)	2.228(2)
150	1.904(1)	2.127(2)	1.792(2)	2.026(1)	2.084(1)	2.222(2)
100	1.905(1)	2.125(2)	1.790(2)	2.026(1)	2.085(1)	2.222(2)
50	1.902(1)	2.126(2)	1.790(2)	2.028(1)	2.083(1)	2.219(2)
3	1.905(1)	2.130(2)	1.790(2)	2.023(1)	2.086(1)	2.217(2)

and W–O distances (table 2) and non-centred cations [10, 13]. The structure parameters at room temperature, obtained from our neutron diffraction study, agree very well with the parameters from [10, 13]. Zn–O distances of 2.025(2), 2.088(2), 2.234(2) Å and W–O distances of 1.784(2), 1.908(2), 2.134(2) Å, belonging to ZnO_6 and WO_6 octahedra, agree closely with the corresponding lengths of 2.026(2), 2.090(2), 2.227(3) Å and 1.790(2), 1.915(2), 2.133(2) Å from [10, 13]. Zn–O and W–O lengths of 2.025(5), 2.094(5), 2.226(5) Å and 1.797(5), 1.915(5), 2.140(5) Å, respectively, as derived from the single crystal x-ray diffraction experiment at room temperature [14] coincide well with those from our study. The angle O2–Zn–O2 between two axial Zn–O distances is 161.44(9)° (similar to 160.96° [10, 13] and 160.56° [14]), significantly less than the ideal 180°. Nevertheless, these distances still lie in the plane containing Zn and bisect the pairs of Zn–O1 and Zn–O2 distances. This is also valid for the WO_6 octahedra with an O1–W–O1 angle of 153.2(1)° (153.11(18)° [10, 13] and 153.2(3)° [14]).

Zn–O and W–O bond distances as derived from neutron diffraction data are summarized in table 2. The three pairs of W–O distances change moderately for temperature changing over the range 3–300 K. Two out of three pairs of Zn–O distances do also not change much (about 0.005 Å in the same temperature range), whereas a much more pronounced dependence, resulting in differences of about 0.02 Å for the data sets collected at 3 and 300 K, was observed for the third pair of Zn–O distances. Figure 3 shows the comparison of temperature dependences of cation–cation distances as derived from the neutron and synchrotron diffraction studies. These are entirely similar. The largest difference of about 0.01 Å between the cation–cation distances was found for the two Zn–Zn distances (figure 3(b)). The most likely cause of these differences is the application of different scattering techniques: the slight discrepancy in the distances obtained from x-ray and neutron data can be due to different interactions of neutrons or x-rays with the atoms. Nevertheless, the deviations are within reasonable limits.

A thorough analysis of the observed isotropic ADP's $B_{\rm iso}$ requires a quantitative treatment, which may be done using the method proposed by Lonsdale [21], where ADP's can be described in the framework of the Debye model by the following relation:

$$B_{\rm iso} = 8\pi^2\left[\frac{145.55T}{M\theta_{\rm D}^2}\phi\left(\frac{\theta_{\rm D}}{T}\right) + A\right]. \qquad (1)$$

The phonon spectrum is approximated by a truncated parabolic function with Debye temperature $\theta_{\rm D}$, M is the atomic mass of the vibrating species and $\phi(\theta_{\rm D}/T)$ is given by

$$\phi\left(\frac{\theta_{\rm D}}{T}\right) = \frac{T}{\theta_{\rm D}}\int_0^{\theta_{\rm D}/T}\left[\frac{x}{{\rm e}^x - 1}\right]{\rm d}x. \qquad (2)$$

The A parameter is related to the ground state energy and is expressed as

$$A = 36.39/(M\theta_{\rm D}). \qquad (3)$$

Due to the presence of a certain amount of static disorder in real materials, the experimentally determined parameter A is usually larger than that calculated from equation (3). Therefore, according to [22], we include into A an additional refinable term corresponding to the sum of static components of the experimental ADP's and uncorrected systematic errors:

$$A = 36.39/(M\theta_{\rm D}) + B_{\rm static}. \qquad (4)$$

The symbols in figure 4 represent the experimental $B_{\rm iso}$ obtained from neutron diffraction data together with error bars plotted *versus* temperature, while the model curves included in the plot corresponds to the least-squares fit results from equations (1)–(4). The refined parameters are listed in table 3. All obtained $B_{\rm static}$ are positive, indicating a certain amount of static disorder in $ZnWO_4$. The averaged mass-weighted value for the Debye temperature is equal to 403(7) K. On the other side, calorimetric measurements were performed on $ZnWO_4$ in the range of 5.11–550 K [23] and the initial Debye temperature $\theta_{\rm D}^{c_p} = 396(8)$ K was derived from the experimental heat capacity data (assuming that the specific heat capacity at constant pressure c_p is approximately equal to that at constant volume c_v in the low-temperature range). The estimates for the Debye temperature from the two different experimental techniques, $\theta_{\rm D}^{c_p} = 396(8)$ K and $\theta_{\rm D}^{B_{\rm iso}} = 403(7)$ K, agree very well.

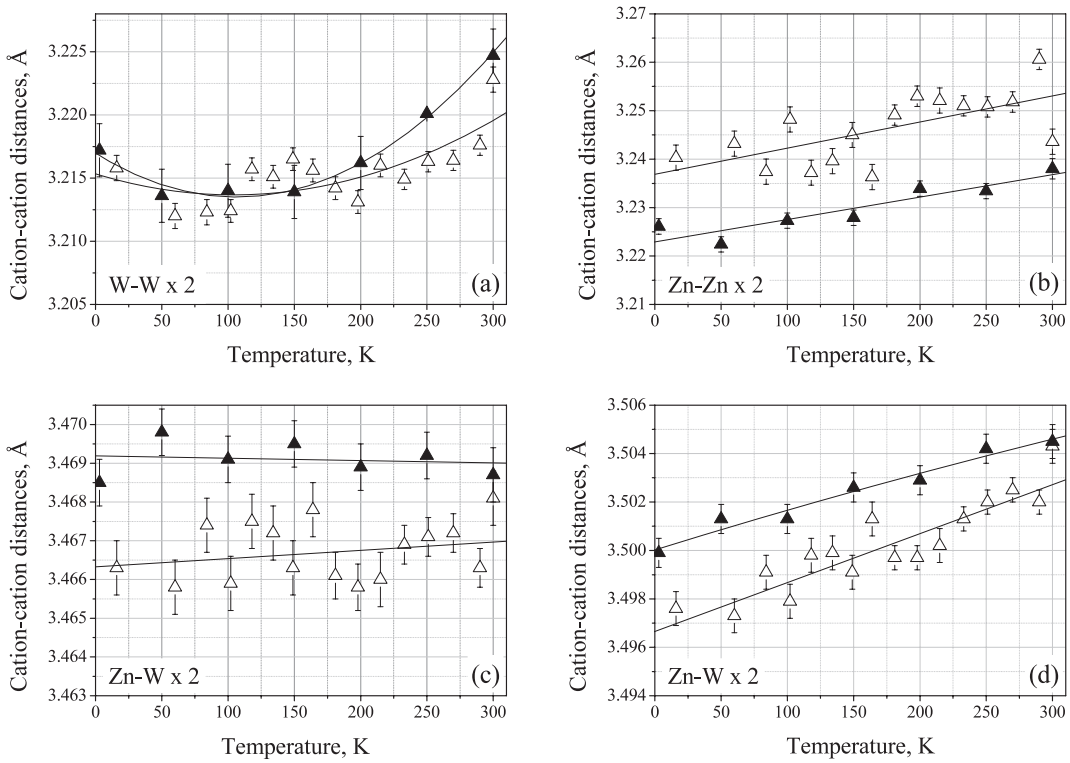

Figure 3. Comparison of the temperature dependencies of cation–cation distances derived from neutron (filled symbols) and synchrotron (empty symbols) diffraction data. The multiplier '×2' denotes the existence of two equivalent distances between cations. The solid lines are guides to the eye.

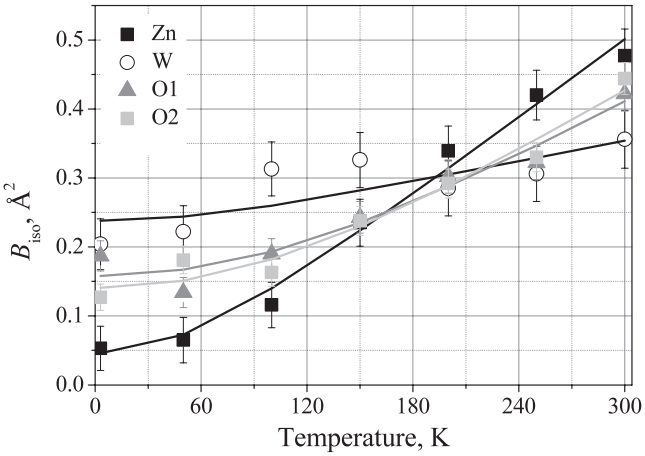

Figure 4. Isotropic ADP's obtained from neutron diffraction as functions of temperature: symbols with error bars show experimental data while solid lines correspond to fits to the data using equations (1)–(4). The fitted parameters are summarized in table 3.

3.2. Thermal expansion in the range of 3–300 K

Figure 5 illustrates the temperature dependencies of the unit-cell dimensions of $ZnWO_4$. The thermal expansions of the three crystallographic axes and the monoclinic angle of $ZnWO_4$ are positive. This 'normal' behaviour is observed throughout the investigated temperature range. Further, the volume thermal expansion was parametrized in the framework of a simple Debye model for the internal energy. Assuming the Grüneisen parameter γ and the bulk modulus K to be temperature independent, the thermal evolution of the cell

Table 3. Parameters resulting from fitting the equations (1)–(4) to the measured ADP's.

Atomic species	θ_D (K)	B_{static} (Å^2)
Zn	300 ± 7	0.04(3)
W	347 ± 8	0.24(4)
O1	692 ± 13	0.15(2)
O2	660 ± 12	0.14(2)

volume at low temperatures can be described within the 1st order Grüneisen approximation as:

$$V(T) = V_0 + \frac{\gamma}{K} U(T), \tag{5}$$

where V_0 is the volume at 0 K and $U(T)$ is the internal energy of the crystal. References [24–26] show that the use of Debye approximation for the internal energy $U(T)$ as in equation (5) provides a reasonable description of the cell volumes. This finding was recently proved in a number of works (see for instance [27, 28]). Thus, taking into account the expression for the internal energy of the crystal in Debye approximation, equation (5) can be rewritten as:

$$V(T) = V_0 + \frac{\gamma}{K}\left[9Nk_BT\left(\frac{T}{\theta_D}\right)^3 \int_0^{\frac{\theta_D}{T}} \frac{x^3\,dx}{e^x - 1}\right], \tag{6}$$

where N is the number of atoms per unit cell. For the $V(T)$ values determined from the x-ray diffraction data, parameters of $V_0 = 131.591(2)$ Å^3, $\gamma/K = 5.2(2) \times 10^{-12}$ Pa^{-1} and $\theta_D = 340(40)$ K are obtained. The same fitting procedure

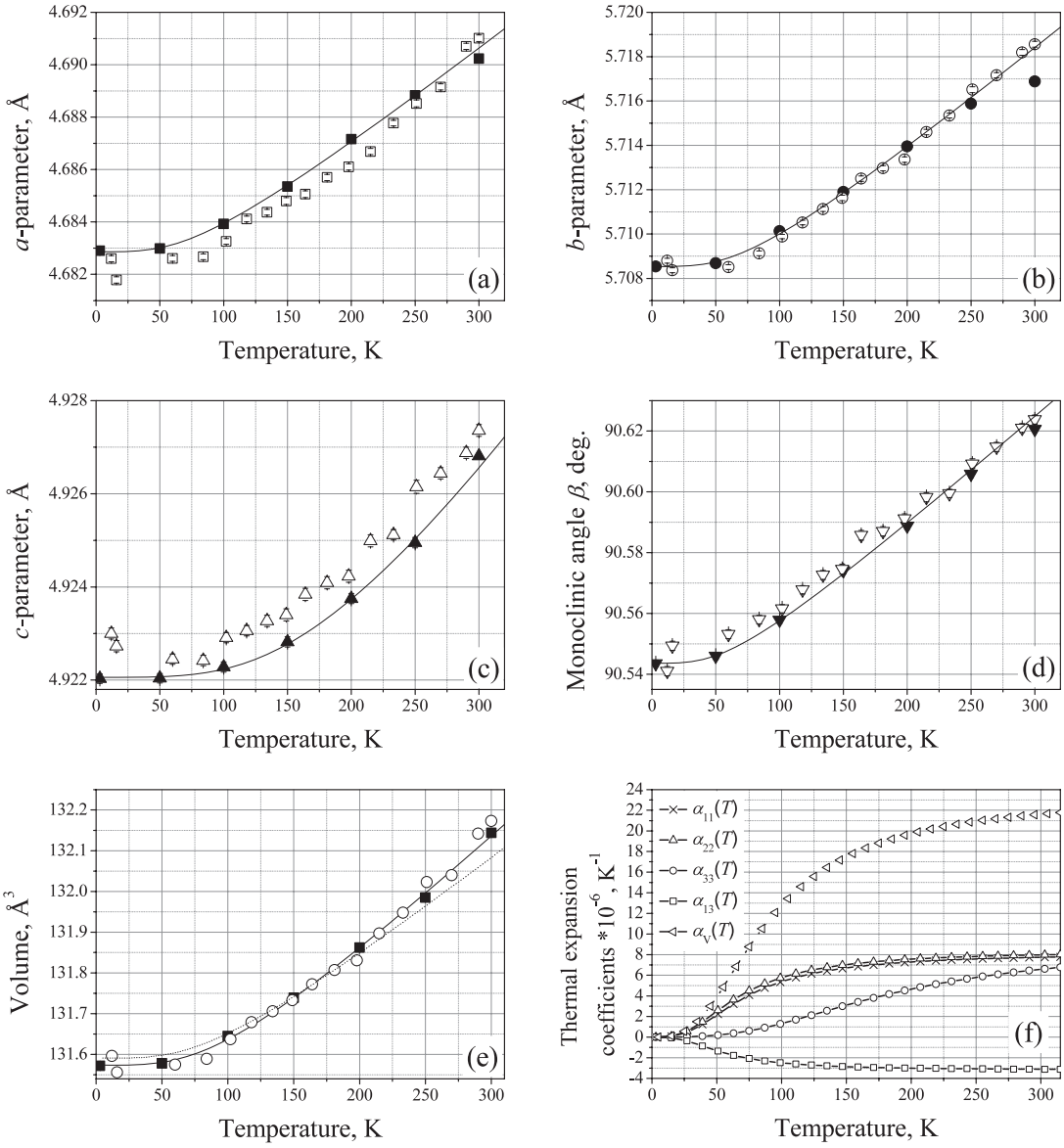

Figure 5. Temperature dependencies of cell dimensions (a)–(e) and thermal expansion coefficients (f) of $ZnWO_4$. Open and solid symbols in (a)–(e) show synchrotron and neutron data, respectively. Lines in figures (a)–(e) display fits according to the 1st order Grüneisen approximation (see text for details).

applied to the neutron data yields $V_0 = 131.574(1)$ Å^3, $\gamma/K = 6.2(1) \times 10^{-12}$ Pa^{-1} and $\theta_D = 370(6)$ K. The results of the fit according to equation (6) are presented in figure 5(e). For the neutron data obtained standard uncertainties were found to be smaller in comparison to the data of synchrotron experiments. This is probably due to a more accurate determination of lattice parameters (because more intense reflections were recorded at higher 2θ) and better temperature stability during the neutron experiment. Both values for the Debye temperature as determined from different experimental data sets obtained either at SPODI (370(6) K) or B2 (340(40) K) are in reasonable agreement with those determined from a specific heat measurements [23] (396(8) K) and from the analysis of the temperature dependence of the experimental ADP's (403(7) K). Assuming the Grüneisen parameter γ being equal to 1 (which is a reasonable value) and taking the parameter $\gamma/K = 6.2(1) \times 10^{-12}$ Pa^{-1} determined from the neutron data, a bulk modulus of 161(3) GPa is estimated. This is in good agreement with the value of 153 GPa determined by ultrasonic phase velocity measurements [29]. Note that our experimental value of 161(3) GPa agrees less (within 14%) with the theoretical bulk modulus of 140 GPa obtained from *ab initio* calculations [30]. Using the γ/K value determined from the synchrotron x-ray data we obtained a bulk modulus of 192 GPa, which agrees less with the literature value of 153 GPa. Since the x-ray data were collected during continuous cooling down to 12 K, such disagreement can be attributed to the effect of temperature during the measurements. The θ_D and K values derived from the analysis of the thermal expansion of $ZnWO_4$, using neutron diffraction data, are consistent with the corresponding literature values, and confirm the validity of the parametrization of the thermal expansion based on the 1st order Grüneisen approximation with Debye approximation for internal energy in this particular case. The neutron diffraction data were used for calculation

Table 4. Parameters resulting from fitting the Debye model (see equations (5)–(7)) to the measured unit-cell parameters.

	x_0 (Å/deg)	x_1 (Pa^{-1})	θ_D (K)
a (Å)	4.682 86(8)	$7.7(2) \times 10^{-14}$	300 ± 10
b (Å)	5.7086(1)	$9.6(2) \times 10^{-14}$	281 ± 11
c (Å)	4.922 06(9)	$7.8(7) \times 10^{-14}$	784 ± 47
β (deg)	90.544(1)	$7.4(2) \times 10^{-13}$	233 ± 11

of the thermal expansion coefficient of $ZnWO_4$, $\alpha_V(T) = \frac{d\ln\{V(T)\}}{dT}$, based on the fitted values V_0, θ_D and γ/K. The temperature dependence of the thermal expansion coefficient is shown in figure 5(f).

The 1st order Grüneisen approximation can be applied equally to individual unit-cell dimensions in the form [27]:

$$x(T) = x_0 + x_1 U(T), \tag{7}$$

where the parameters x_0, x_1 and θ_D are obtained from the fit. The results from fitting equation (7) to the lattice parameters are plotted as solid lines in figures 5(a)–(d), and the corresponding model parameters are compiled in table 4. It can be seen from figure 5 that these models give very good representations of the temperature behaviour of all cell dimensions. Using the refined parameters obtained from fitting the temperature dependence of the lattice parameters (table 4), we calculated the magnitude of the thermal expansion coefficients as a function of temperature. The anisotropic thermal expansion of a monoclinic crystal with b as unique axis is given by a second rank tensor $\alpha_{(ij)}$ (see [31] and references therein):

$$\alpha_{11}(T) = \frac{1}{a_0}\frac{da}{dT} + \frac{d\beta}{dT}\cot\beta \tag{8}$$

$$\alpha_{22}(T) = \frac{1}{b_0}\frac{db}{dT} \tag{9}$$

$$\alpha_{33}(T) = \frac{1}{c_0}\frac{dc}{dT} \tag{10}$$

$$\alpha_{13}(T) = \frac{1}{2}\left[\cot\beta\left(\frac{1}{a_0}\frac{da}{dT} - \frac{1}{c_0}\frac{dc}{dT}\right) - \frac{d\beta}{dT}\right]. \tag{11}$$

The components $\alpha_{11}(T)$, $\alpha_{22}(T)$, $\alpha_{33}(T)$ and $\alpha_{13}(T)$ in the range of 3–300 K are plotted in figure 5(f). The anisotropy of the thermal expansion is apparent for $ZnWO_4$: $\alpha_{11}(T)$ and $\alpha_{22}(T)$ are similar in magnitude and appear to saturate close to 8×10^{-6} K^{-1}, whereas $\alpha_{33}(T)$ exhibits a lower value without reaching saturation. $\alpha_{13}(T)$ is negative and exhibits comparatively small changes at temperatures higher than 120 K. Figure 5(f) illustrates that $\alpha_{11}(T)$ practically equals $\alpha_{22}(T)$. This experimental finding is readily attributed to the features of the $ZnWO_4$ structure. As can be seen from figure 2, each chain of ZnO_6 octahedra is corner-linked in the x–y plane to four chains of WO_6 octahedra and *vice versa*, i.e., the isotropic expansion in the x–y plane can be explained by equivalent corner linkages between rigid octahedral units in the ⟨110⟩ directions. The expansion along the c-axis—the direction where zigzag chains are formed by either edge-sharing ZnO_6 or edge-sharing WO_6 octahedra—is lower than along the a- and b-directions.

3.3. High-temperature investigation by thermal analysis and crystal structure at 1423 K

Before performing high-temperature neutron diffraction, the $ZnWO_4$ was characterized by simultaneous thermal analysis. The two different measurements were carried out in air in a Al_2O_3 crucible with heating–cooling rates of 10 and 5 K min^{-1} up to a maximum of 1573 K. A clear change of the base line and the appearance of yellow needles in the final product could be attributed to a reaction of the sample with corundum. Therefore we performed a second measurement in Pt-crucibles with a heating–cooling rate of 5 K min^{-1} up to 1573 K. The $ZnWO_4$ sample melts at 1478 K (peak onset, peak maximum at 1486 K) and, subsequently, solidifies at 1442 K on cooling, thus demonstrating some temperature hysteresis which is clearly depending on the heating rate and the crucible material (in Al_2O_3 the hysteresis is significantly smaller). In order to evaluate the structural information for the $ZnWO_4$ at high temperatures, neutron powder diffraction data were collected at 1423 K. In agreement with the thermal analysis data, the analysis of the high-temperature diffraction pattern does not reveal any phase changes and the Rietveld refinement was based on the monoclinic $P2/c$ symmetry as it was at low temperatures. The final result of the fit is displayed in figure 1(c) while refined values of structural parameters of $ZnWO_4$ at 1423 K are summarized in table 1.

4. Conclusions

In this work we carried out comprehensive structural studies of $ZnWO_4$ over a wide temperature range, using synchrotron x-ray and neutron diffraction techniques. No phase transitions were observed in $ZnWO_4$ with wolframite structure from 3 K up to the melting point at 1486 K. The interatomic distances and angles, as well as the atomic displacement parameters behave quite normally. It has been shown that the low-temperature evolution of the $ZnWO_4$ lattice volume can be modelled fairly well in framework of the 1st order Grüneisen approximation with a Debye approximation for the internal energy. Despite the simplicity of this parametrization, implying a temperature-invariant γ and K, the Debye temperature and the bulk modulus obtained from this description of the lattice expansion agree well within reasonable limits with the literature values, thus giving strong support for the suitability of the model for $ZnWO_4$. The magnitudes of the thermal expansion tensor coefficients as a function of temperature were calculated and it is demonstrated how the pronounced anisotropic behaviour in the expansivity of $ZnWO_4$ can be attributed to the specific structural features.

Acknowledgments

This work was supported in part by a grant from the Royal Society (London) and the Ukrainian Ministry of Education and Science (Projects 'Segnet' and 'Tern'). The neutron powder diffractometer SPODI is operated in the frame of the 'Instrumentation at large-scale facilities for condensed matter research' programme of the Bundesministerium für Bildung und Forschung under grant no. 03FU7DAR. HASYLAB@DESY is acknowledged for allocation of the beamtime.

Table A.1. Structural parameters of $ZnWO_4$ resulted from simultaneous fits to neutron and synchrotron diffraction data at 300 K. The space group is $P2/c$ (No. 13), $Z = 2$.

a (Å), b (Å), c (Å), β (deg.)	4.6906(1)	5.7182(1)	4.9269(1)	90.621(1)
Atom, site	x/a	y/b	z/c	B_{iso} (Å^2)
Zn, 2f	0.5	0.6858(2)	0.25	0.56(4)
W, 2e	0	0.1814(2)	0.25	0.40(1)
O1, 4g	0.2159(5)	0.8937(4)	0.4386(6)	0.35(5)
O2, 4g	0.2577(6)	0.3728(6)	0.4007(7)	0.48(5)
Synchrotron data: R_p (%), R_{wp} (%), χ^2		4.01	5.30	15.4
Neutron data: R_p (%), R_{wp} (%), χ^2		5.06	6.26	2.83

Appendix. Results of simultaneous diffraction data treatment

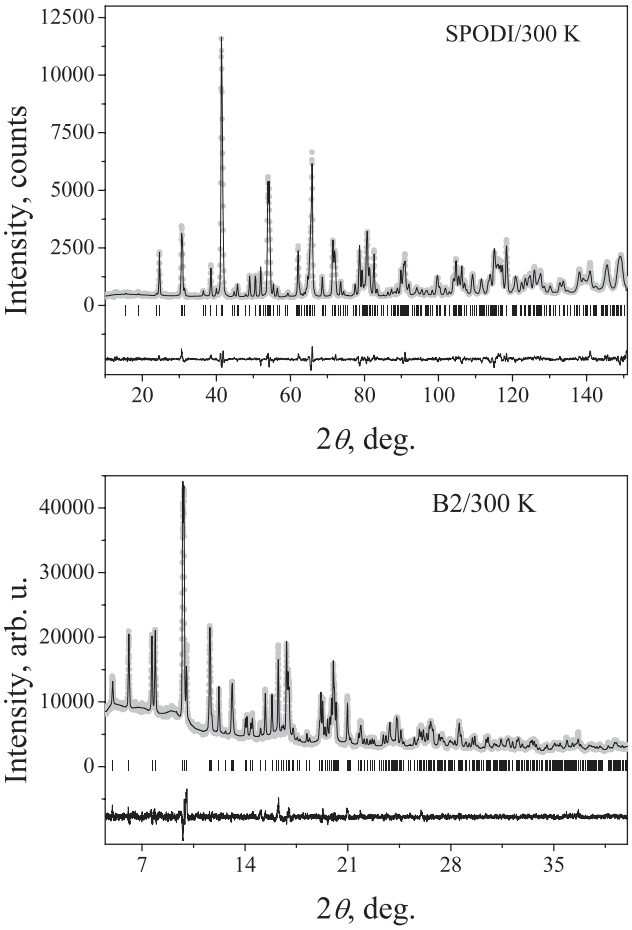

Figure A.1. Neutron and synchrotron diffraction patterns of $ZnWO_4$ treated simultaneously.

References

[1] Kraus H, Mikhailik V B, Ramachers Y, Day D, Hutton K B and Telfer J 2005 *Phys. Lett.* B **610** 37–44

[2] Danevich F A, Kobychev V V, Nagorny S S, Poda D V, Tretyak V I, Yurchenko S S and Zdesenko Yu G 2005 *Nucl. Instrum. Methods* A **544** 553–64

[3] Mikhailik V B and Kraus H 2006 *J. Phys. D: Appl. Phys.* **39** 1181–91

[4] Mikhailik V B, Kraus H, Miller G, Mykhaylyk M S and Wahl D 2005 *J. Appl. Phys.* **97** 083523

[5] Kraus H, Mikhailik V B, Vasylechko L, Day D, Hutton K B, Telfer J and Prots Yu 2007 *Phys. Status Solidi* a **204** 730–6

[6] Danevich F A, Henry S, Kraus H, McGowan R, Mikhailik V B, Shkulkova O G and Telfer J 2008 *Phys. Status Solidi* a **205** 335–9

[7] Nagornaya L L, Dubovik A M, Vostretsov Y Ya, Grinyov B V, Danevich F A, Katrunov K A, Mokina V M, Onishchenko G M, Poda D V, Starzhinskiy N G and Tupitsyna I A 2008 *IEEE Trans. Nucl. Sci.* **55** 1469–72

[8] Kraus H, Danevich F A, Henry S, Kobychev V V, Mikhailik V B, Mokina V M, Nagorny S S, Polischuk O G and Tretyak V I 2009 *Nucl. Instrum. Methods* A **600** 594–8

[9] Filipenko O S, Pobedimskaya E A and Belov N V 1968 *Sov. Phys.—Crystallogr.* **13** 127

[10] Schofield P F, Knight K S and Cressey G 1996 *J. Mater. Sci.* **31** 2873–7

[11] Schofield P F and Redfern S A T 1993 *J. Phys. Chem. Solids* **54** 161–70

[12] Redfern S A T, Bell A M T, Henderson C M B and Schofield P F 1995 *Eur. J. Mineral.* **7** 1019–28

[13] Schofield P F, Knight K S, Redfern S A T and Cressey G 1997 *Acta Crystallogr.* B **53** 102–12

[14] Dahlborg M A and Svensson G 1999 *Acta Chem. Scand.* **53** 1103–9

[15] Knapp M, Baehtz C, Ehrenberg H and Fuess H 2004 *J. Synchrotron Radiat.* **11** 328–34

[16] Ihringer J and Küster A 1993 *J. Appl. Crystallogr.* **26** 135–7

[17] Knapp M, Joco V, Baehtz C, Brecht H H, Berghaeuser A, Ehrenberg H, von Seggern H and Fuess H 2004 *Nucl. Instrum. Methods* A **521** 565–70

[18] Hoelzel M, Senyshyn A, Gilles R, Boysen H and Fuess H 2007 *Neutron News* **18** 23–6

[19] Roisnel T and Rodriguez-Carvajal J 2001 *Mater. Sci. Forum* **378–381** 118

[20] Lyon W G and Westrum E F Jr 1974 *J. Chem. Thermodyn.* **6** 763–80

[21] Lonsdale K 1962 Temperature and other modifying factors *International Tables for X-Ray Crystallography* vol III ed C H MacGillavry and G D Riek (Birmingham: Kynoch Press) p 232

[22] Argyriou D N 1994 *J. Appl. Crystallogr.* **27** 155–8

[23] Landee C P and Westrum E F Jr 1975 *J. Chem. Thermodyn.* **7** 973–6

[24] Vočadlo L, Knight K S, Price G D and Wood I G 2002 *Phys. Chem. Miner.* **29** 132–9

[25] Sayetat F, Fertey P and Kessler M 1998 *J. Appl. Crystallogr.* **31** 121–7

[26] Wood I G, Knight K S, Price G D and Stuart J A 2002 *J. Appl. Crystallogr.* **35** 291–5

[27] Fortes A D, Wood I G, Vočadlo L, Brand H E A and Knight K S 2007 *J. Appl. Crystallogr.* **40** 761–70
[28] Senyshyn A, Trots D M, Engel J M, Vasylechko L, Ehrenberg H, Hansen T, Berkowski M and Fuess H 2009 *J. Phys.: Condens. Matter* **21** 145405
[29] Pisarevskii Yu V, Silvestrova I M, Voszka R, Peter A, Földvari I and Janszky J 1988 *Phys. Status Solidi* a **107** 161–4
[30] Errandonea D, Manjón F J, Garro N, Rodríguez-Hernández P, Radescu S, Mujica A, Muñoz A and Tu C Y 2008 *Phys. Rev.* B **78** 054116
[31] Paufler P and Weber T 1999 *Eur. J. Mineral.* **11** 721–30